Interferometry Based Radar Imaging by Leveraging Cellular Communication Networks

Husheng Li

***Abstract*—The communication signals sent from base stations (BSs) in 5G networks can be leveraged for radar sensing, by exploiting the illumination by data communication signals. The technique of interferometry imaging, which has been extensively used in radio astronomy, is used as the mathematical framework for the radar imaging, by exploiting the distances among cellular BSs. To address the near field imaging, different from the far field in radio astronomy, the hyperbola family of constant-distance-difference trajectory is derived. Numerical simulations are carried out for demonstrating the proposed algorithms.**

I. Introduction

Beyond providing high-rate and low-latency data communications, the 5G signaling facilitates radar sensing, by leveraging the communication infrastructure and signal. An illustration is shown in Fig. 1, where a base station (BS) sends out a beam that illuminates an area, and multiple BSs receive the reflected signal for computational imaging in the multiaccess edge computing (MEC) device. A BS can focus its beam open angle to a narrow scope and thus distinguish close objects for imaging, similarly to the spotlight-mode synthetic aperture radar (SAR) [1] except for the mobility. One motivation is the precise positioning of user equipments (UEs) in 5G systems, up to the precision of 3m (vertical, and horizontal indoors) and 10m (horizontal outdoors), in 3GPP TR 38.857 [2]. An indoor positioning experiment has achieved the precision of 30cm in Qualcomm [3]. Essentially, the spatial resolution of antenna array and beamforming is dependent on the distance between array elements. Then, in principle, the different BSs in 5G communication network can provide distant separations of antennas, thus forming a virtual antenna array and achieving finer spatial resolutions. A motivating example is the first successful imaging of black hole in 2019 [4], which is 550 light years away from the earth and requires an angle resolution of 20 microarcseconds. It leverages 8 radio astronomy telescopes distributed over the earth and works in the millimeter wave (mmWave) band of wavelength 1mm. Motivated by the imaging of black hole, the communication network can work in a similar manner to improve the sensing sensitivity, by exploiting the distances between the BSs in the network.

In this paper, we propose to use the mathematical principle of interferometry in the blackhole imaging [4], for the purpose of radar imaging by reusing the 5G BSs and communication signals. It is well known that, in optics, interferometry can be used to detect tiny deformations, by exploiting the short wavelength of high frequency electromagnetic (EM) wave [5]. This sensitivity enhances the spatial resolution and discloses fine angular structures, such that astronomists can 'see' the distant blackholes. Note that the proposed scheme is not confined to the mmWave band and could also be used in sub-6GHz bands. Although we will adopt the framework of interferometry used in radio astronomy, the principle cannot be applied directly. The reason is that, in radio astronomy, the BSs are in motion (due to the orbital revolution and spin of the earth), thus forming many distant 'virtual' antennas. In a contrast, the BSs in 5G systems are typically stationary, and thus cannot form virtual BSs. Thanks to the dense deployment of BSs in 5G networks, even the fixed BSs could be sufficient for the task of imaging. Another challenge is that far field can be safely assumed in radio astronomy, due to the large distance to the target. However, in the distance of signal propagation in 5G networks, the source usually generates a near field, thus requiring new approaches.

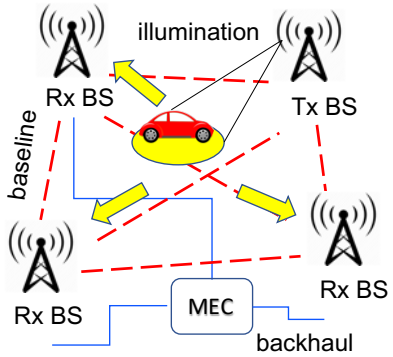

Fig. 1. An illustration of 5G network based imaging.

Note that the proposed interferometry based sensing scheme is more suitable for outdoor scenarios, where the targets are illuminated by transmitting BSs. In suburban areas with much less reflectors, line of sight (LOS) can be established between the illuminated area and the receiving BSs, and sub-6GHz band signal can be used without the dense deployment. To our best knowledge, this is the first work to apply the sensing technique in astronomy in 5G networks, which is promising for significantly improving the sensing capability as a 'bonus', since no extra hardware infrastructure is needed.

The remainder of this paper is organized as follows. The related studies are introduced in Section II. The system model, as well as the mathematical framework of interferometry, will be explained in Section III. Then, imaging algorithms for cases

H. Li is with the Department of Electrical Engineering and Computer Science, the University of Tennessee (email: husheng@eecs.utk.edu). This work was supported by the National Science Foundation under grants 2052780, 2135286, 2109295 and 2128455.

of far field and near field will be discussed in Sections IV and V, respectively. Numerical results and conclusions are provided in Sections VI and VII, respectively.

II. Related Studies

In this section, we introduce existing studies related to this paper. Communication signals are reused for sensing in the following aspects: (a) Positioning and Ranging: mmWave communication signal is used for positioning based on signal features [6]. Due to its wide deployment, the Wi-Fi band signal has been substantially used for sensing various targets [7]. (b) Imaging: 60GHz mmWave communication signals have been used for target imaging [8]. The approaches using communication signals for sensing, which are the most similar to our proposed interferometry scheme, are compared, which includes the time difference of arrivals (TDOA) [9] and passive radar (e.g., the Cooperative Passive Coherent Location (CPCL) [10]). Compared with these approaches, the proposed interferometry approach does not need active signal from the target (like in TDOA and AOA) and does not need LOS reference signal (like in CPCL), thus minimizing the cost and prerequisite of the system.

III. System Model and VLBI

In this section, we introduce the system model, and the principle of VLBI that is used in radio astronomy.

A. System Model

We consider a communication network with N BSs. The positions of the BSs, denoted by $\{\mathbf{r}_n\}_{n=1,...,N}$, could be arbitrary, unless mentioned otherwise. Each BS is equipped with N_r receive antennas, which could be reused for transmission (in a half-duplex mode) or are used for only receiving (in a full-duplex mode). For single carrier case, we denote the carrier frequency and wavenumber by f_c and k, respectively. For the case of K sub-carriers, the corresponding wavenumbers are denoted by $\{k_i\}_{i=1,...,K}$. For simplicity, we assume that the UEs do not participate in the imaging procedure, since it incurs too much overhead to send the raw data to the MEC through the air interface, and its precise position can hardly be obtained.

B. Principle of VLBI

We introduce the principle of VLBI, which is used in radio astronomy and will be employed in our communication network based imaging. The spatial resolution enhancement in the black hole imaging is based on VLBI [11]. We consider a simple example, where two BSs with distance D receive the signals reflected from a certain object, from incident angle θ. The signal received at the left BS is denoted by $V(t)$. The correlation of the received signals is then given by

$$r(\theta,\tau)=\lim_{T\to\infty}\frac{1}{2T}\int_{-T}^{T}V(t)V(t-\tau)dt, \tag{1}$$

where the time delay $\tau=\tau_g+\tau_i$, $\tau_g=D\sin\theta/c$ is the geometric propagation time delay and τ_i is the intentional artificial delay added to the signal. The procedure of correlation is similar to the interference of two coherent light beams propagating through different paths. It is shown that, if the signal has a Gaussian PSD with mean v_0 and variance σ, the correlation function is given by (ref. Eq. (2.11) in [11])

$$r(\theta,\tau) \quad = \quad e^{-2\left(\frac{\pi D\sigma}{c}\sin\theta+\tau_i\right)^2}\cos\left(\frac{2\pi v_0 D\sigma}{c}\sin\theta+\tau_i\right). \tag{2}$$

The correlation function $r(\theta,\tau)$ is illustrated for a fixed τ. When the distance D is large, the exponential term in (2) decays very fast and the cosine term has a very short period, thus resulting in very high resolution in the angle θ.

IV. Imaging Algorithm: Far Field

In this section, we study the communication-signal-based imaging algorithm using the principle of interferometry, in the far field. For simplicity, we first study the bi-static case and then extend to generic multiple-BS case.

A. Received Signal

We first consider two BSs and a single-tone signal with wavenumber k. We denote by $\mathbf{D}$ the baseline vector between the two BSs (from antenna N_r of BSs 1 to antenna 1 of BS 2), such that $\|\mathbf{D}\|=D$. Note that we index the antennas such that the incident wave arrives in the order of antennas 1, 2, ..., N_r of BS 1 and then those of BS 2. Consider an illuminated region Ω, whose brightness at direction $\mathbf{s}$ is denoted by $I(\mathbf{s})$.

We assume that the antennas of the two BSs are aligned along directions $\mathbf{l}_1$ and $\mathbf{l}_2$, with a half-wavelength spacing. Then, the received signal at antenna n ($n=1,...,N_r$) and BS i ($i=1,2$) is given by $V_{in}=V_{i1}e^{-j(n-1)k\mathbf{l}_i\cdot\mathbf{s}}$, where we assume that the amplitudes of the received signals at different antennas are the same. Suppose that BS 1 receives the signal earlier. Then, we have $V_{21}=V_{1N_r}e^{-jk\mathbf{D}\cdot\mathbf{s}}$.

B. Fine AoA Estimation

Similarly to the VLBI, we also calculate the correlation function between the received signals at the two BSs. However, in our context, each BS has multiple antennas, which have the capability of angular resolution by using traditional beamforming. Therefore, we carry out traditional receive beamforming at each BS, namely computing the following linear combination:

$$x_i(\mathbf{s}_0,\mathbf{s})=\sum_{n=1}^{N_r}V_{in}e^{-j(n-1)k\mathbf{l}_i\cdot\mathbf{s}_0}, \qquad i=1,2, \tag{3}$$

where $\mathbf{s}_0$ is the desired direction. It is easy to show that, when the signal AOA is $\mathbf{s}$, x_i equals

$$x_i(\mathbf{s}_0,\mathbf{s})=V_{i1}\exp\left(j\pi\Delta_r\delta\theta_i(N_r-1)\right)\frac{\sin(\pi L_r\delta\theta_i)}{\sin(\pi L_r\delta\theta_i/N_r)}, \tag{4}$$

where L_r is the length of antenna array, and $\delta\theta_i$ is defined as $\delta\theta_i=\sin^{-1}(\mathbf{l}_i\cdot\mathbf{s}_0)-\sin^{-1}(\mathbf{l}_i\cdot\mathbf{s})$, which indicates the gap between the directions. When $\delta\theta$ is sufficiently small, we have

$$x_i(\mathbf{s}_0,\mathbf{s})\approx V_{i1}\frac{\sin(\pi L_r\delta\theta_i)}{\sin(\pi L_r\delta\theta_i/N_r)}, \tag{5}$$

In the above discussion, $\{x_i\}_{i=1,2}$ are denoted by their phasor forms. Now we take the oscillation $e^{2\pi f_c t}$ into account, where we consider a single carrier frequency f_c. Then, we

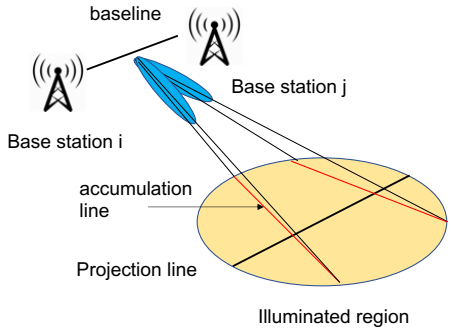

Fig. 2. An illustration of single-baseline imaging.

calculate the correlation with an arbitrarily added delay τ, namely

$$\begin{aligned} R(\tau) &= E[Re\left(x_1(t)x_2^*(t+\tau)\right)] \\ &= \prod_{i=1}^{2} \frac{\sin(\pi L_r \delta\theta_i)}{\sin(\pi L_r \delta\theta_i/N_r)} \cos\left(kD\sin\theta - 2\pi f_c\tau\right), \end{aligned} \quad (6)$$

where $\theta = \sin^{-1}(\mathbf{D}\cdot\mathbf{s})$. We set $2\pi f_c\tau = kD\cos(\theta_0)$, where $\theta_0 = \sin^{-1}(\mathbf{D}\cdot\mathbf{s}_0)$. Then we have

$$\cos\left(kD\sin\theta - 2\pi f_c\tau\right) \approx \cos\left(kD\sin\delta\theta\cos\theta_0\right), \quad (7)$$

where $\delta\theta = \theta - \theta_0$. Thus $R(\tau)$ can also be written as $R(\delta\theta)$.

In the planar case, it is easy to show that $\delta\theta_1 = \delta\theta_2 = \delta\theta$. Therefore, we have

$$R(\delta\theta) \approx \prod_{i=1}^{2} \frac{\sin(\pi L_r\delta\theta)}{\sin(\pi L_r\delta\theta/N_r)} \cos\left(u\sin\delta\theta\right), \quad (8)$$

where $u = kD\cos\theta_0$ is called the spatial frequency [11]. We observe that, when $\delta\theta = 0$, $R(\delta\theta)$ is maximized. When $\delta\theta$ increases, but still keeping small, the value of $R(\delta\theta)$ decreases rapidly. This provides substantial spatial resolution. In typical scenarios, $L_r \ll D$. Therefore, the spatial resolution mainly stems from the long distance D between the two BSs.

C. Imaging Algorithm

Each baseline, or BS pair, can leverage the fine angle resolution to scan the source intensity along the baseline direction. However, the sources along the same direction are mixed in the estimated intensity, as illustrated in Fig. 2, thus being indistinguishable. To distinguish the source intensities, one has to seek help from multiple frequencies of signal, by exploiting the spatial-frequency spectrum and Fourier transform. For continuous spectrum case, we assume that the signal passband is $[k_l, k_h]$ (in terms of wavenumber). Then, at BS i, we calculate the following correlation:

$$x_i(\mathbf{s}_0, r) = \sum_{n=1}^{N_r} \int_{k_l}^{k_h} e^{j(n-1)k\mathbf{l}_i\cdot\mathbf{s}_0} V_{in}(w,t) e^{jkr} dk, \quad (9)$$

where the scalar r is the range of the desired source point along the direction $\mathbf{s}_0$. For practical OFDM signaling, the above signal can be approximated by

$$x_i(\mathbf{s}_0, r) = \sum_{n=1}^{N_r}\sum_{l=1}^{K} e^{j(n-1)k_l\mathbf{l}_i\cdot\mathbf{s}_0} \cdot V_{in}^l(t) e^{jk_l r}, \quad (10)$$

where V_{in}^l is the signal at subcarrier l, antenna n and BS i. Given the above analysis, we feed the correlation in (9) into the interferometer. When the bandwidth is sufficiently large, it is expected that the output is proportional to $\|\rho(\mathbf{s}_0, r)\|^2$. By changing the values of $\mathbf{s}_0$ and r, we can obtain the source intensities at different positions of the source, thus completing the task of imaging.

Algorithm 1 Single-baseline imaging

1: Determine the angle step $\delta\theta$, range stage δr, numbers of steps N_a (angle) and N_r (range)
2: **for** $n_1 = 1, ..., N_a$ **do**
3: Determine angle $\theta = (n_1 - N_a/2)\delta\theta$ and direction $\mathbf{s}$.
4: Determine the range $r = (n_2 - N_f/2)\delta r$.
5: Using (10) to compute the signals x_i, $i = 1, 2$. Calculate the correlation of x_1 and x_2. The norm of the output is set as the intensity of the pixel $(\mathbf{s}, r)$
6: **end for**
7: Carry out inversion to obtain the image reconstruction.

V. Imaging Algorithm: Near Field

In this section, we consider the near field case, in which the assumption that there is a single incident angle is no longer valid. The proposed algorithm is based on the detailed analysis on the equal-distance-difference (EDD) curve family.

A. Single Baseline

We first consider a single baseline. We realize that the capability of spatial resolution in interferometry is due to the traveling time difference incurred by the distance of receiving antennas. In interferometry, this time difference is not directly estimated; instead, it is obtained from the correlation of the signals received at different antennas.

1) Analysis of Fringe - Single Reflection Point: Consider two receiving antennas, whose coordinates are $(-x_0, 0)$ and $(x_0, 0)$, as well as a monochromatic (with wavenumber k) point source at position (x, y). The received signals at the two antennas are given by $s_i(t) = A_i\cos(wt + kd_i)$, $i = 1, 2$, where d_i is the distance from the source to the i-th antenna. The correlation function is then given by

$$E[s_1(t)s_2(t+\tau)] = A_1A_2\cos(w\tau + k(d_1 - d_2)), \quad (11)$$

whose peaks are located at $\tau_l = \frac{l\pi - k(d_1-d_2)}{w}$, $l \in \mathbb{N}$. When the peaks $\{\tau_l\}_{l\in\mathbb{N}}$ are well estimated, we obtain the estimation on the distance difference $\delta d = d_1 - d_2$:

$$\delta d_m = cE\left[\frac{l\pi}{w} - \tau_l\right] + \frac{m\lambda}{2}, \quad (12)$$

where m indicates the uncertainty of multiples of half wave length.

Suppose that the source point is located in the upper half plane. Then, the points satisfying the distance difference in (12) are the upper part of the hyperbola $\frac{x^2}{a_m^2} - \frac{y^2}{b_m^2} = 1$, where

$$\begin{cases} a_m = \frac{\delta d_m}{2} \\ b_m = \sqrt{x_0^2 - a_m^2} \end{cases} . \tag{13}$$

This hyperbola trajectory has also been discovered in the study of time difference of arrival (TODA) [12]. The trajectories of the hyperbola EDD family, given the interferometry fringe.

2) Multiple Source Points and Multiple Subcarriers: Suppose that there are multiple, say L, incoherent point sources, whose distance differences to the baseline of two BSs are δd_1, ..., δd_L. Assume that $\delta d_1 \bmod(\lambda/2) \neq ... \neq \delta d_L \bmod(\lambda/2)$; otherwise, they cannot be distinguished by the baseline. The received signals from these sources are mixed and thus yield

$$Re\left(E[s_1(t)s_2(t+\tau)]\right) = \sum_{l=1}^{L} A_l^2 \cos(w(\tau - \tau_l)), \tag{14}$$

where $\tau_l = \frac{\delta d_l}{c}$. We assume that the amplitudes of the signals from the same source and received at the two BSs are the same.

Our task is to decouple the mixture in (14) and estimate A_i and τ_l. To this end, we calculate the Fourier transform of $R(\tau) = E[s_1(t)s_2(t+\tau)]$ (which equals the cross power spectral density (PSD) of $s_1(t)$ and $s_2(t)$) and obtain

$$P(v) = \sum_{l=1}^{L} A_l^2 \left(e^{-jw\tau_l}\delta(v-w) + e^{jw\tau_l}\delta(v+w)\right). \tag{15}$$

From the cross PSD P, we obtain the complex scalar $\tilde{A}(w) = \sum_{l=1}^{L} A_l^2 e^{-jw\tau_l}$, by taking the peak in the positive frequency.

For a single frequency w, it is impossible to decouple the signals from the single scalar $\tilde{A}$. Hence, we seek help from the multi-subcarrier structure and consider the K subcarriers:

$$\tilde{A}(w_i) = \sum_{l=1}^{L} A_l^2 e^{-jw_i\tau_l}, i = 1, ..., K. \tag{16}$$

We can consider (16) as the mixture of multiple sinusoidal functions with frequencies $\{\tau_l\}_{l=1...,L}$, if we consider the frequency w_i as time. Therefore, the time delays (as frequencies), as well as the corresponding EDD curve families, can be obtained from discrete Fourier transform (DFT) over the K values of $\tilde{A}(w_i)$, $i = 1, ..., L$, namely picking the significant peaks in the DFT.

B. Multiple Baselines for Imaging

Now, we consider multiple baselines and the corresponding imaging, given the results on single baseline.

1) Fine Positioning: We first study the fine positioning of a source point using the above analysis of interferometry fringes. We assume that a rough range of the source point has been obtained, say, using phase arrays at different BSs. We consider more than 2 BSs, thus forming more than one baselines. By computing the fringes of different baselines, the families of EDD hyperbolas are determined. If the illuminated region is sufficiently small, then there is a unique hyperbola in each EDD family corresponding to each baseline, intersecting the rough region. The intersection point of the hyperbolas corresponding to different baselines is determined to be the position of the point source.

2) Imaging: Using the above analysis, for a given baseline, we decouple the signals and obtain the powers of signals with different distance differences, denoted by $\{P_i, \delta d_i\}_{i=1,..,L}$, where L is the number of distance difference values. Due to the assumption of incoherent source, each power p_i equals the accumulation of the signal power on the EDD hyperbolas:

$$P_i = \int_{\mathcal{P}(\delta d_i)\cap\Omega} p(\mathbf{r}) d\mathbf{r}, \tag{17}$$

where $\mathcal{P}(\delta d_i)$ denotes the EDD hyperbolas corresponding to the distance difference δd_i.

To reconstruct the image, we first discretize the region of the image into S sub-regions, such that the powers of points in the same subregion are approximately identical. The power-subregion tuples are denoted by $\{p_i, \Omega_i\}_{i=1,...,S}$. Then, we use Q baselines, each recovering the power-difference pairs $\{P_{qi}, \delta d_{qi}\}_{q=1,...,Q, i=1,...,L}$ from the above analysis. Using (17), we attain the following equations:

$$P_{qi} = \sum_{j=1}^{S} p_j P(\mathcal{P}_q(\delta d_i), \Omega_i),\ q = 1, ..., Q, i = 1, ..., L, \tag{18}$$

where $P(\mathcal{P}_q(\delta d_i), \Omega_i)$ is the proportion of the hyperbola $\mathcal{P}_q(\delta d_i)$ falling in the subregion Ω_i. When there are sufficiently many measurements P_{qi}, the equation can be solved to obtain the image intensities $\{p_i\}_{i=1,...,S}$.

VI. Numerical Results

In this section, we provide numerical results to demonstrate the proposed algorithms.

A. Far Field Case

Note that the far field condition can hardly be satisfied. Consider the 2.5GHz band and two BSs that are only 20 meters away. The distance of target for far field needs to be more than $2D^2/\lambda$, which is 6.4km away. At such a distance, the reflected 5G signal will be too weak to be sensed, when the path loss and ground absorption are taken into account. In the mmWave band, the distance qualifying a far field analysis will be even much longer. Figure 3 shows the angular resolution based on two-BS interferometry. We consider the 60GHz band and both cases of single antenna and 400 antennas per BS. The corresponding antenna array is 0 and 1 meter long, respectively. The distance between the two BSs ranges from 10 meters to 200 meters. The upper plot shows the fast improvement on the angular resolution (degrees) with respect to different BS distances. Moreover, the two curves ($L_r = 0$ and $L_r = 1$, recall that L_r is the length of antenna array) overlap exactly, which implies that the antenna array at each BS does not contribute to the fine resolution of angle. However, the lower plot shows the function $R(\delta\theta)$, which is periodic, for monochromatic sources. Therefore, the antenna arrays at different BSs are still necessary, for they can locate the coarse scope of the AOA, which removes the ambiguity of the interferometry. We also plotted the angular resolution of a

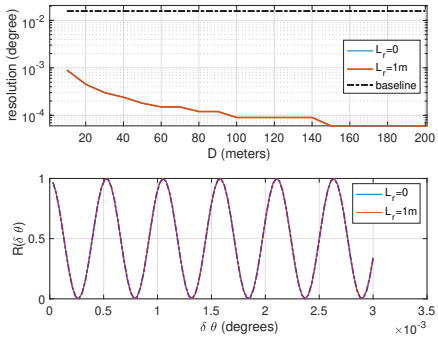

Fig. 3. Angle resolution based on two-BS interferometry

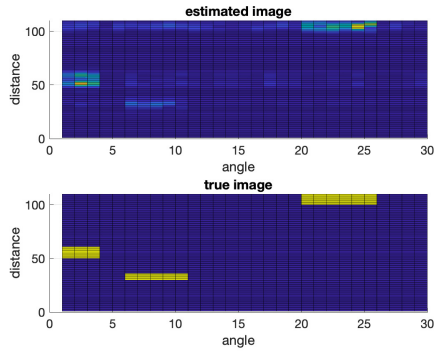

Fig. 4. Reconstruction of significant reflectors

single antenna array with 400 antennas, which is much coarser than the interferometry.

We applied Algorithm 1 to sense an arc-area of 30 degrees by 11 meters. 1024 sub-carriers in the 2.5GHz band are considered. For simplicity, we ignore the noise and path loss. We assume three significant reflectors in this area, as illustrated in the lower half of Fig. 4. The estimated image is shown in the upper part of Fig. 4. It is observed that the shapes of the three reflectors have been approximately reconstructed, despite some artificial ripples due to the limited signal bandwidth and thus the limited resolution.

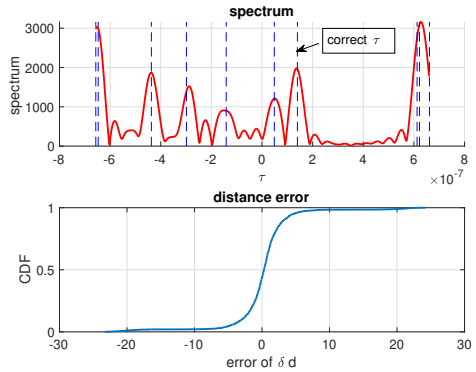

Fig. 5. Estimation of distance difference in the near field

B. Near Field Case

For the near field case, there is no baseline for comparison, since most single-array processing schemes consider only the far field case. We tested the algorithm for identifying multiple targets in (15) and (16), by considering the 2.5GHz band and 1024 subcarriers, with a total bandwidth of 130MHz. For each realization, 10 significant targets are randomly distributed within a 500m$\times$500m region. The upper image in Fig. 5 shows the spectrum peaks, as well as the true values of τ indicated by the vertical dotted lines. We observe that almost all significant peaks correspond to certain targets, while some targets that are too close to each other are confused within the same peak. The estimation error cumulative distribution function (CDF) of the distance difference is plotted in the lower image of Fig. 5, where the error is symmetric and is mainly within 5 meters. The missed detection rate of target is 31.2%.

VII. Conclusions

In this paper, we have proposed to use the interferometry of received communication signals at different BSs for imaging the environment, by exploiting the distances between different BSs. The difference between the interferometry schemes in communications and radio astronomy has been identified. Both far field and near field have been studied.

References

[1] R. J. Sullivan, *Microwave Radar: Imaging and Advanced Concepts*. Artech House, 2000.

[2] G. T. 38.857, "Study on nr positioning enhancements," ., 2020.

[3] Q. Inc., "What key technology inventions will drive the 5g expansion?" 2020. [Online]. Available: https://www.qualcomm.com/news/onq/2020/07/03/what-key-technology-inventions-will-drive-5g-expansion

[4] T. E. H. T. Collaboration, "First m87 event horizon telescope results. i. the shadow of the supermassive black hole," *The Astrophysical Journal Letters*, 2019.

[5] E. Hecht, *Optics*. Pearson, 2017.

[6] F. Lemic, J. Martin, C. Yarp, D. Chan, V. Handziski, R. Brodersen, G. Fettweis, A. Wolisz, and J. Wawrzynek, "Localization as a feature of mmwave communication," in *2016 International Wireless Communications and Mobile Computing Conference (IWCMC)*. IEEE, 2016, pp. 1033–1038.

[7] K. Qian, C. Wu, Z. Yang, Y. Liu, and K. Jamieson, "Widar: Decimeter-level passive tracking via velocity monitoring with commodity wi-fi," in *Proc. of ACM Mobihoc*, 2017.

[8] Y. Zhu, Y. Zhu, B. Y. Zhao, and H. Zheng, "Reusing 60Ghz radios for mobile radar imaging," in *Proceedings of the 21st Annual International Conference on Mobile Computing and Networking*, 2015, pp. 103–116.

[9] S. Dwivedi, R. Shreevastav, F. Munier, J. Nygren, I. Siomina, Y. Lyazidi, D. Shrestha, G. Lindmark, P. Ernstrom, E. Stare, S. M. Razavi, S. Muruganathan, G. Masini, A. Busin, and F. Gunnarsson, "Positioning in 5G networks," *arxiv*, 2021.

[10] R. S. Thoma, C. Andrich, G. D. Galdo, M. Dobereiner, M. A. Hein, M. Kaske, G. Schafer, S. Schieler, C. Scheider, A. Schwind, and P. Wendland, "Cooperative passive coherent location: A promising 5g service to support road safety," *IEEE Communications Magazine*, vol. 57, no. 9, pp. 86–92, 2019.

[11] A. R. Thompson, J. M. Moran, and G. W. S. Jr., *Interferometry and Synthesis in Radio Astronomy, 3rd edition*. Springer, 2017.

[12] F. Gustafsson and F. Gunarsson, "Positioning using time-difference of arrival measurements," in *Proc. of IEEE International Conference on Acoustics, Speech, and Signal Processing, 2003. Proceedings. (ICASSP '03)*. IEEE, 2003.